# Cell relay-delivery improves targeting and therapeutic efficacy in tumors

Ye Feng [a,b,1], Qianqian Liu [a,1], Yi Li [a,1], Yang Han [a,c], Meng Liang [a], Hao Wang [a], Qing Yao [a,c], Yuli Wang [a], Meiyan Yang [a], Zhiping Li [a], Wei Gong [a], Yang Yang [a,*], Chunsheng Gao [a,**]

[a] State Key Laboratory of Toxicology and Medical Countermeasures, Beijing Institute of Pharmacology and Toxicology, Beijing, 100850, PR China
[b] Hubei University of Science and Technology, Xianning, 437100, PR China
[c] School of Traditional Chinese Medicine, Shenyang Pharmaceutical University, Shenyang, 110016, PR China

## ABSTRACT

Cell-mediated drug delivery system (CDDS) has shown great potential for cancer therapy. However, a single cell-mediated drug delivery mechanism has not generally been successful, particularly for systemic administration. To augment the antitumor therapy efficacy, herein, we propose a strategy of cell relay-delivery for the use of artificially damaging/aging erythrocytes to hitchhike on circulating monocytes/macrophages for intratumoral accumulation of anticancer drugs. This biomimetic relay-delivery strategy was derived from the manner in which circulating monocytes/macrophages in body specifically engulf damaged/senescent erythrocytes and actively transmigrate into the tumor bulk. The strategy elegantly combines the natural functions of both cells, which therefore provides a new perspective to challenge current obstacles in drug delivery. According to the strategy, we developed biotinylated erythrocyte-poly (lactic-co-glycolic acid) (PLGA) nanoparticle hybrid DDSs (bE-NPs) using avidin-biotin coupling. In such a system, biotinylated erythrocytes can mimic the natural property of damaged/senescent erythrocytes, while PLGA NPs are capable of encapsulating anticancer drugs and promoting sustained drug release. Anticancer drugs can effectively target tumor sites by two steps. First, by using biotinylated erythrocytes as the carrier, the drug-loaded PLGA NPs could be specifically phagocytized by monocytes/macrophages. Second, by taking advantage of the tumor-tropic property of monocytes/macrophages, the drug-loaded PLGA NPs could be efficiently transported into the tumor bulk. After encapsulating vincristine (VIN) as the model drug, bE-NPs exhibited the most favorable antitumor effects *in vitro* and *in vivo* by the cell relay-delivery effect. These results demonstrate that the cell relay-delivery provides a potential method for improving tumor treatment efficacy.

## 1. Introduction

Cell-mediated drug delivery system (CDDS) which employs specific cells as drug vehicles to delivery drugs to targeted sites has shown great potential for several diseases therapy, such as cancer [1]. Compared with conventional DDSs, CDDSs offer several advantages, such as their inherent targeting delivery ability, biocompatibility, and low immunogenicity. In body, monocytes/macrophages by nature can actively home and extravasate through the tight vascular wall into the tumor bulk along chemoattractant gradients towards tumors [2,3]. Taking advantage of their natural behavior, *ex vivo*-generated monocytes/macrophages has been exploited as Trojan Horses for the tumor targeting of therapeutic agents [4]. Unfortunately, the viability of the

reinjected *ex vivo* loading of monocytes/macrophages with therapeutic agents was significantly reduced, and only less than 5% of those retained their intrinsic migratory ability, extremely limiting their tumor-targeting effectiveness [5]. Moreover, this strategy suffers from high cost, the risk of *ex vivo* contamination, as well as insufficient quantities of harvested monocytes/macrophages.

As an alternative strategy, direct *in situ* loading of monocytes/macrophages with therapeutic agents is more advantageous towards clinical practice. To achieve *in situ* loading of circulating monocytes/macrophages with therapeutics, many attempts have focused on drug loaded nanoparticles (NPs) which could be directly engulfed by the mononuclear phagocyte systems (MPS) [6]. While the natural tendency of circulating monocytes/macrophages to more readily internalize NPs

could be beneficial for designing monocytes/macrophages-hitchhiked delivery systems, the resident macrophages' penchant for internalizing NPs is still an important challenge in developing circulating monocytes/macrophages-hitchhiked delivery systems [7,8]. While this ability might be exploited to target macrophages in liver cancer, delivery of NPs to circulating monocytes/macrophages must compete with avid internalization by hepatic and splenic macrophages (e.g. Kupffer cells and dendritic cells) [9,10]. In order to improve monocytes/macrophages selectivity over resident macrophages, some researchers reported the use of targeting ligands modified NPs to facilitate preferential delivery to monocytes/macrophages via ligand-receptor in interaction [11]. In these ligand-modified DDSs, however, the targeting moieties distribute uniformly on the NPs surface, with only a small proportion participating in the interaction with monocytes/macrophages, causing limited recognition ability as well as incomplete utilization of ligand materials [12]. Moreover, problems with some synthetic materials still exist and even cause toxicology issues. Nevertheless, the development of more generalizable and efficient methods to specifically hitchhike on circulating monocytes/macrophages remains challenging.

In order to effectively achieve *in situ* loading of circulating monocytes/macrophages with therapeutics, their intrinsic phagocytic behavior to specifically engulf some endogenous waste materials in blood stream can be exploited [13]. Among these endogenous waste materials, damaged/senescent erythrocytes are one of the most promising biological vehicles. It is well known that most of the damaged/senescent erythrocytes in circulation are specifically eliminated by monocytes/macrophages [14,15]. Phagocytosis of erythrocytes arises either from the binding of autoantibodies and subsequent recognition by Fc receptors on the monocytes/macrophages surface or by opsonization of erythrocytes by plasma proteins that can mediate phagocytosis, such as those belonging to the complement system [16]. Interestingly, the artificially damaging/aging erythrocytes can also mimic the natural property of damaged/senescent erythrocytes very well. Moreover, the artificially damaging/aging erythrocytes can be easily obtained in large numbers by chemical modifications [17]. This source is easy for scaling up and economic preparation compared with other endogenous waste materials, such as apoptotic bodies. Due to their unique properties, the artificially damaging/aging erythrocytes may constitute excellent biological vehicles for circulating monocytes/macrophages-hitchhiked anticancer drug loading.

On the basis of natural behaviors of these cells, herein, we propose a strategy of cell relay-delivery for the use of artificially damaging/aging erythrocytes to hitchhike on circulating monocytes/macrophages for intratumoral accumulation of anticancer drugs. This biomimetic delivery strategy elegantly combines the natural functions of both cells, i.e. the natural monocytes/macrophages-targeted behavior of damaged/senescent erythrocytes and the natural tumor-homing tendency of monocytes/macrophages, which therefore provides a new perspective to challenge current obstacles in drug delivery. According to the strategy, we developed biotinylated erythrocyte-poly (lactic-co-glycolic acid) (PLGA) nanoparticle hybrid DDSs (bE-NPs) using avidin-biotin coupling. The molecular binding affinity of avidin to biotin has been widely utilized in biological research and in the development of DDSs [18]. In this study, erythrocytes were modified with biotin, followed by incorporation of an avidinated form of PLGA NPs to the erythrocyte surface with high efficiency. Notably, the membrane modification of erythrocytes with biotin can produce an artificially damaging/aging effect for erythrocytes [19]. The biotinylation renders the complement subcomponent C3b in serum to deposit on the erythrocytes' membrane [20]. Given that C3b receptors are highly expressed on the surface of monocytes/macrophages, C3b-opsonized erythrocytes can be readily engulfed by monocytes/macrophages [21,22]. Thus, biotinylated erythrocytes can mimic the natural property of damaged/senescent erythrocytes. The PLGA NPs themselves are capable of encapsulating large amounts of anticancer drugs and having a characteristic sustained-release

mechanism. Conjugation through the avidin-biotin bridge usually provides stronger attachments; therefore, it prevents the detachment of drug carrier PLGA NPs during biotinylated erythrocyte migration. Being carried by biotinylated erythrocytes, the drug-loaded PLGA NPs could be rapidly phagocytized by circulating monocytes/macrophages. Based on the tumor-tropic property of monocytes/macrophages, the drug-loaded PLGA NPs could be efficiently transported into the inner region of tumor. After encapsulating vincristine (VIN), the research data demonstrated that the VIN-loaded bE-NPs were more effective than VIN-loaded nanoparticles at inhibiting tumor growth in tumor-bearing animal models. Based on these findings, bE-NP was expected to induce a potent and translatable cell relay-delivery platform for further exploring the application of cell-mediated carriers in oncotherapy.

## 2. Materials and methods

### 2.1. Materials

NH$_2$-PEG$_{2000}$-PLGA (actic/glycolic acid ratio (75/25) and 0.55–0.75 dL/g inherent viscosity) were provided by Xi'an ruixi Biological Technology Co., Ltd (Xi'an, China). Vincristine (VIN) was purchased from Min Sheng Pharmaceutical Co. (Zhejiang, China). All chemicals were of reagent grade and were obtained from Sigma-Aldrich, unless otherwise stated.

Both Walker-256 cells and RAW264.7 cells were purchased from the National Infrastructure of Cell Line Resource (Beijing, China). Walker-256 cells were maintained in RPMI-1640 medium (Gibco) supplemented with 10% fetal bovine serum (FBS) (Gibco) and 1% penicillin–streptomycin (Gibco). RAW264.7 cells were maintained in culture medium consisting of dulbecco's modified eagle's medium (DMEM) (Gibco) supplemented with 10% FBS and 1% penicillin–streptomycin. The cells were maintained in a 37 °C humidified incubator in a 5% CO$_2$ atmosphere.

Female Sparague-Dawley rates (190–210 g) were provided by Vital River Laboratories (Beijing, China). All animal experiments were complied with the code of ethics in research, training and testing of drugs issued by the Animal Care and Use Ethics Committee in Beijing Institute of Pharmacology and Toxicology.

### 2.2. Synthesis of streptavidin-PEG$_{2000}$-PLGA

Streptavidin-PEG$_{2000}$-PLGA was synthesized by an amidation reaction [23]. Briefly, to form active ester functional groups for amine coupling, streptavidin was activated by NHS (N-hydroxysuccinimide) and EDC (1-ethyl-3-[3-dimethylaminopropyl]carbodiimide HCl) at room temperature. For the coupling to PEG$_{2000}$-PLGA, an excess of activated streptavidin (2 eq.) was added to the NH$_2$-PEG$_{2000}$-PLGA, and reacted at room temperature. Excess reactant and unconjugated streptavidin was removed by extensive dialysis in a 300K MWCO CE ester membrane.

### 2.3. Preparation of nanoparticles

Streptavidin-PEG$_{2000}$-PLGA nanoparticles (s-NPs) were prepared using the O/W emulsion method, as previously reported. Streptavidin-PEG$_{2000}$-PLGA (20 mg) and VIN (3 mg) or hydrophobic probe (DIR, or FITC, 100 μL) were added to 2 mL of a mixture of acetone. After being completely dissolved, it was poured into 5 mL of 1% (w/w) PVA solution. Then, the mixture was stirred in open air for 4 h to obtain VIN-loaded s-NPs or hydrophobic probe-tagged s-NPs.

### 2.4. Characterization of nanoparticles

The mean diameter and particle distribution of the s-NPs were measured by dynamic light scattering (DLS) (Litesizer 500, Anton Parr, Austria). The morphology of streptavidin-NPs was characterized by

transmission electron microscopy (TEM) (HITACHI, H-7650, Japan).

## 2.5. Preparation of bE-NPs

Whole blood was collected from the orbital sinus of Sprague-Dawley (SD) rats. Then, erythrocytes were separated form whole blood by centrifugation at 4 °C, 600 × g for 5 min and washed twice at 4 °C with PBS. Biotinylation of erythrocytes was carried out by a previously reported method [19]. In brief, 5 mL of succinylated bovine serum albumin (BSA) was first added to the erythrocyte suspension and shaken for 10 min at 37 °C. Then, amounts of NHS-biotin were added to the mixture, followed by incubation at 37 °C for 1 h. To determine the optimal amount of biotin in the formulations, different concentrations of NHS-biotin were compared. The biotinylated erythrocytes were recovered by centrifugation at 250 × g and washed three times with ice-cold PBS to remove unconjugated reactants. To prepare bE-NPs, amounts of s-NPs (equivalent to NHS-biotin) were incubated with the resulting biotinylated erythrocytes for 30 min at 37 °C to ensure the complete binding between biotin and streptavidin. The bE-NPs obtained by the above manner were finally centrifuged and washed with ice-cold PBS to remove unconjugated reactants. The s-NPs assembly to biotinylated erythrocytes were confirmed using scanning electron microscopy (SEM) (HITACHI, S-4800, Japan) and confocal laser scanning microscopy (CLSM) (UltraVIEW Vox, PerkinElmer, USA).

## 2.6. Extent of modification and binding efficiency

To determine the substitution level of biotin molecules per erythrocyte, biotinylated erythrocytes and FITC-streptavidin (Nanjing Xinfan Biological Technology Co., Ltd, Nanjing, China) were incubated at 37 °C for 30 min. After removal of unattached FITC-streptavidin, the relative levels of NHS-biotin-streptavidin-FITC binding on erythrocytes were determined by flow cytometry (FCM) (BD FACSCalibur, USA) using FITC fluorescence.

To determine the efficiency of s-NPs anchored on biotinylated erythrocytes, biotinylated erythrocytes and FITC-tagged s-NPs were incubated at 37 °C for 30 min. After removal of unattached FITC-tagged s-NPs, the relative levels of FITC-tagged s-NP binding on biotinylated erythrocytes were determined by FCM using FITC fluorescence.

## 2.7. In vitro release profile

The dialysis method was used to study the *in vitro* release of VIN from the VIN-loaded s-NPs or bE-NPs. Dialysis bags (MW. Cutoff: 14 kDa) with 1 mL of VIN-loaded s-NPs or bE-NPs were directly immersed into 30 mL of PBS (0.1 M, pH 7.4) at 37 °C. At preset time points, 800 μL aliquots were withdrawn from the solution and the same volume of PBS was added. The VIN in the obtained samples was measured using HPLC as reported previously [36].

## 2.8. C3b in serum depositing and binding on the surface of erythrocytes

bE-NPs or biotinylated erythrocytes were pretreated with serum at 37 °C for 1 h. Equivalent healthy erythrocytes was treated as a control at the same condition. After the pretreatment, healthy erythrocytes, biotinylated erythrocytes and bE-NPs were respectively collected and incubated with monoclonal antibodies recognising C3b (mAb 2B10B9B2, Hycult Biotech, PA, USA), followed by staining with Alexa Fluor 488-conjugated Goat Anti-Mouse IgM secondary antibody (ab150121, Abcam). FCM was used for quantification of these C3b on the surface of erythrocytes at ex/em of 495/519 nm.

## 2.9. Cytotoxicity

To measure the cellular toxicity of empty bE-NPs, RAW264.7 cells were seeded into 96-well plates ($1 \times 10^4$/well) in DMEM at 37 °C in a 5% $CO_2$ atmosphere. After incubation for 24 h, the cells were treated with empty bE-NPs, empty s-NPs or empty biotinylated erythrocytes and were incubated for another 72 h. For the cytotoxity of drug-loaded bE-NPs to RAW264.7 cells as carriers, equivalent stoichiometric free VIN and VIN-loaded bE-NPs (100 ng/mL of VIN) were respectively incubated with RAW264.7 cells for 3 h. After incubation, the un-phagocytosed free VIN or VIN-loaded bE-NPs were discarded. And the celles were kept in fresh media for another 0–24 h. At the end of each time point (0, 2, 4, 8, 12, 16 and 24 h), cell viability was evaluated with 3- (4, 5- dimethyl- 2- thiazolyl)-2, 5- diphenyl-2 -H- tetrazolium bromide (MTT assay). The morphology of RAW264.7 cells were observed and photographed under the optical microscope at the time point of 24 h before MTT assay.

## 2.10. Hemolysis assay of empty bE-NPs

Two hundred microliters of erythrocytes from healthy rat were seeded into 96-well plates. Next, the cells were incubated with PBS (Negative control), Triton-X (Positive control), empty bE-NPs, empty s-NPs or empty biotinylated erythrocytes. After incubation for 6 h at 37 °C, the cells were centrifuged and then the supernatants of the sample were measured at 414 nm using a microplate reader (Elx-800; Bio-Tek Instruments, USA) [24] . The equation for the rate of hemolysis is as follow:

$$\text{Hemolysis (\%)} = (OD_{Sample} - OD_{Negative})/(OD_{Positive} - OD_{Negative}) \times 100\%$$

## 2.11. In vivo preliminary safety evaluation

Healthy rats were randomly divided into three groups (n = 6) and were treated with 5% glucose (control) and empty bE-NPs via the tail vein. In the empty bE-NPs groups, the blood was taken from rats and the bE-NPs were prepared and then returned back to the rats. The daily body weight was recorded every day. On day 7, these rats were sacrificed, and samples of the heart, liver, spleen, lung, and kidney were collected and routinely stained by HE.

## 2.12. Macrophage uptake

Equivalent stoichiometric FITC-tagged bE-NPs and FITC-tagged s-NPs were respectively incubated with excessive RAW264.7 cells for 3 h. These samples were pretreated with rat serum or PBS-BSA (PBS containing 2 mg mL$^{-1}$ BSA) (37 °C, 1 h) before incubation with the RAW264.7 cells. After incubation, the free bE-NPs or s-NPs were discarded, and RAW264.7 cells were collected and stained with Hoechst 33258 for 20 min to visualize the cell nuclei. Finally, the stained cells were washed and kept in PBS for qualitative analysis by CLSM [25].

## 2.13. In vitro efficiency of bE-NPs phagocytosed by macrophages

Excessive RAW264.7 cells were incubated with serum-pretreated bE-NPs at 37 °C for 0–24 h. After incubation, the suspensions containing RAW264.7 cells and bE-NPs were immediately analyzed by FCM. The un-phagocytosed bE-NPs were gated and distinguished from RAW264.7 cells according to SSC and FSC based on the different dimensions between erythrocytes and macrophages.

## 2.14. In vitro tumor accumulation

Walker-256 tumor spheroids were established as follows: $2 \times 10^3$ cells in 100 μL of culture media were plated onto a 48-well plate pre-coated with 50 μL of 2% low melting point agarose. For RAW264.7 cell-hitchhiked FITC-tagged bE-NPs, FITC-tagged bE-NPs were first treated with rat serum for 1 h at 37 °C and then incubated with RAW264.7 cells for another 3 h at 37 °C. The spheroids were incubated with RAW264.7

cell-hitchhiked FITC-tagged bE-NPs, FITC-tagged bE-NPs or FITC-tagged s-NPs for 6 h at 37 °C. The tumor spheroids were rinsed with PBS before being transferred to chambered coverslips and then analyzed by CLSM. Z-stack images were obtained by scanning the tumor spheroid step by step. The scanning began from the top of the spheroid to the equatorial plane.

### 2.15. In vivo imaging

Female SD rats received a subcutaneous injection of Walker-256 cells (0.1 mL, $1 \times 10^7$) in the right front flank. These tumor bearing rats were used for tumor targeting evaluation. Briefly, blood was taken from rats and the DIR-tagged bE-NPs were prepared as described above and returned back to these rats via tail vein injection. The rats in the control group were administered with DIR-tagged s-NPs. 12 h after i.v. injection, *in vivo* imaging was performed using IVIS® Spectrum-CT. Fluorescent signals were quantified using Living Image® software (Caliper, Alameda, CA). After *in vivo* imaging, the rats were sacrificed by cervical dislocation, and the major organs, including the heart, liver, spleen, lung, and kidney, were excised and imaged.

### 2.16. Immunofluorescence staining

The subcutaneous Walker-256-bearing rats were administered FITC-tagged bE-NPs or FITC-tagged s-NPs via tail vein injection. In the FITC-tagged bE-NPs group, the blood was taken from rats and the FITC-tagged bE-NPs were prepared as described above. After 12 h postinjection, these rats were anesthetized and perfused with saline and 4% paraformaldehyde. The tumors were harvested and fixed in 4% paraformaldehyde and then dehydrated with sucrose solution for 24 h and embedded in OCT (Sakura, Torrance, CA, USA). The tumors were cut into 5 mm by frozen sectioning and subjected to fluorescence microscope after staining with DAPI (blue) for the distribution of FITC-tagged bE-NPs (green) in tumor. For analyzing the tumor-infiltrated macrophages, sections were incubated with Ribbit monoclonal antibodies recognising CD11b (ab133357, Abcam) and Mouse monoclonal antibodies recognising CD68 (ab201340, Abcam), followed by staining with AlexaFluor 568-conjugated Goat Anti-Ribbit IgG secondary antibody (shown in red) and AlexaFluor 647-conjugated Goat Anti-Mouse IgG secondary antibody (shown in violet). The images were captured by fluorescence microscope and presented as visions on the site with a tumor penetration depth of 2 mm.

### 2.17. Concentration of VIN in solid tumors

Nine rats were randomly divided into three groups and intravenously administered with free VIN, VIN-loaded bE-NPs or VIN-loaded s-NPs at a dose of 1.0 mg/kg VIN (diluted to 0.2 ml by physiological saline), respectively. In the VIN-loaded bE-NPs group, the blood was taken from rats and the VIN-loaded bE-NPs were prepared as described above. 12 h after i.v. injection, rats were sacrificed and the tumors were collected and stored at −20 °C until analysis. VIN was extracted from the tumors by protein precipitation [26]. For VIN concentration detection, the samples were homogenized in 3-fold volumes of distilled water with the homogenate pretreated via a protein precipitation procedure using vinblastine sulfate as the I.S., and the supernatant following centrifugation was subjected to LC-MS/MS analysis as described previously [27].

### 2.18. In vivo antitumor efficacy

The subcutaneous Walker-256-bearing rats were injected in the tail vein with 5% glucose (control), 1.0 mg/kg free VIN, VIN-loaded bE-NPs and VIN-loaded s-NPs on the 6th, 9th, 12th and 15th day. In the VIN-loaded bE-NPs group, blood was taken from the rats and the VIN-loaded bE-NPs were prepared as described above. Six animals were

randomly selected from every group, and the tumor volume and animal body weight were measured. The estimated tumor volume was calculated using the formula: volume $(mm^3) = (length \times width^2)/2$. Then, blood from the subcutaneous Walker-256-bearing rats was collected via the orbit and assayed. Next, these animals were sacrificed, and samples of the heart, liver, spleen, lung, and kidney were collected and routinely stained by HE. Hemogram analysis and histological staining of organs were performed to evaluate the *in vivo* safety properties of the VIN-loaded bE-NPs. The remaining animals of all groups (n = 6) were used in the survival test. The time between the tumor transplantation day and the animal sacrifice day was used to calculate the survival time. Then, the Kaplan-Meier survival curve of each group was plotted.

### 2.19. Immunohistochemical analysis of tumors

After the achievement of tumor inhibition data, the animals were sacrificed and their tumors collected. Each tumor was fixed in 10% formalin buffer for 24 h, embedded in paraffin, and then sectioned (5 μm thick). CD31 antibody was used in immunohistochemical study [28]. The tumor tissue was observed using a light microscope (Olympus, Japan) and photographed.

### 2.20. Statistical analysis

All data are presented as the means ± standard deviation (SD). The data were analyzed using one-way ANOVA coupled with Dunnett post hoc analysis to carry out multigroup comparison. Comparison between two groups was accomplished via an unpaired two-tailed student's t-test. The probability of survival was estimated by the Kaplan-Meier method and compared by the log-rank test. The relative fluorescence intensities and immunohistochemistry stainings were assessed using the Image J software of at least 3 samples per group with 3 different sections per sample. $p < 0.05$ indicated a statistically significant difference.

## 3. Results and discussion

### 3.1. Preparation and characterization of bE-NPs

The preparation scheme for bE-NPs is illustrated in Fig. 1A. To stably attach drug carrier NPs to the surface of erythrocytes, in this study, we exploited a facile yet robust approach using a simple avidin-biotin interaction. First, we prepared the streptavidin form of NPs in which the surface of nanoparticles included biotin-reactive streptavidin headgroups, using the O/W emulsion method. After encapsulating VIN, the VIN-loaded s-NPs had a diameter of 157 ± 0.87 nm (Fig. S1) with a polydispersity index of 0.103 ± 0.045, which indicated a narrow size distribution. As shown in Fig. S2, the VIN-loaded s-NPs were relatively monodispersed with a well-defined spherical morphology. In addition, the TEM image demonstrated that the particle sizes were similar to those determined using a laser particle analyzer. As VIN is a hydrophobic drug, which is easily entrapped in PLGA, the encapsulation efficiency (EE) and drug loading capacity (DL) of VIN-loaded s-NPs were relatively high (EE, 93.45 ± 0.85%; DL, 5.36 ± 1.02%).

To link VIN-loaded s-NPs to erythrocytes via the surface avidin-biotin, biotinylation of erythrocytes were carried out by attachment with NHS-biotin. To screen the optimized amounts of NHS-biotin, erythrocytes were incubated with different concentrations of NHS-biotin. As shown in Fig. S3, when increasing amounts of NHS-biotin (from 100 μg to 300 μg) were used, there was a significant increase in the substitution level of biotin molecules per erythrocyte. However, when continually increasing the amount to 400 μg, there was no remarkable enhancement in the substitution level of biotin than that of the 300 μg amount (P > 0.05). This could be due to the surface saturation phenomenon of erythrocytes. Therefore, the 300 μg of NHS-biotin concentration was chosen for biotinylation throughout the experiment.

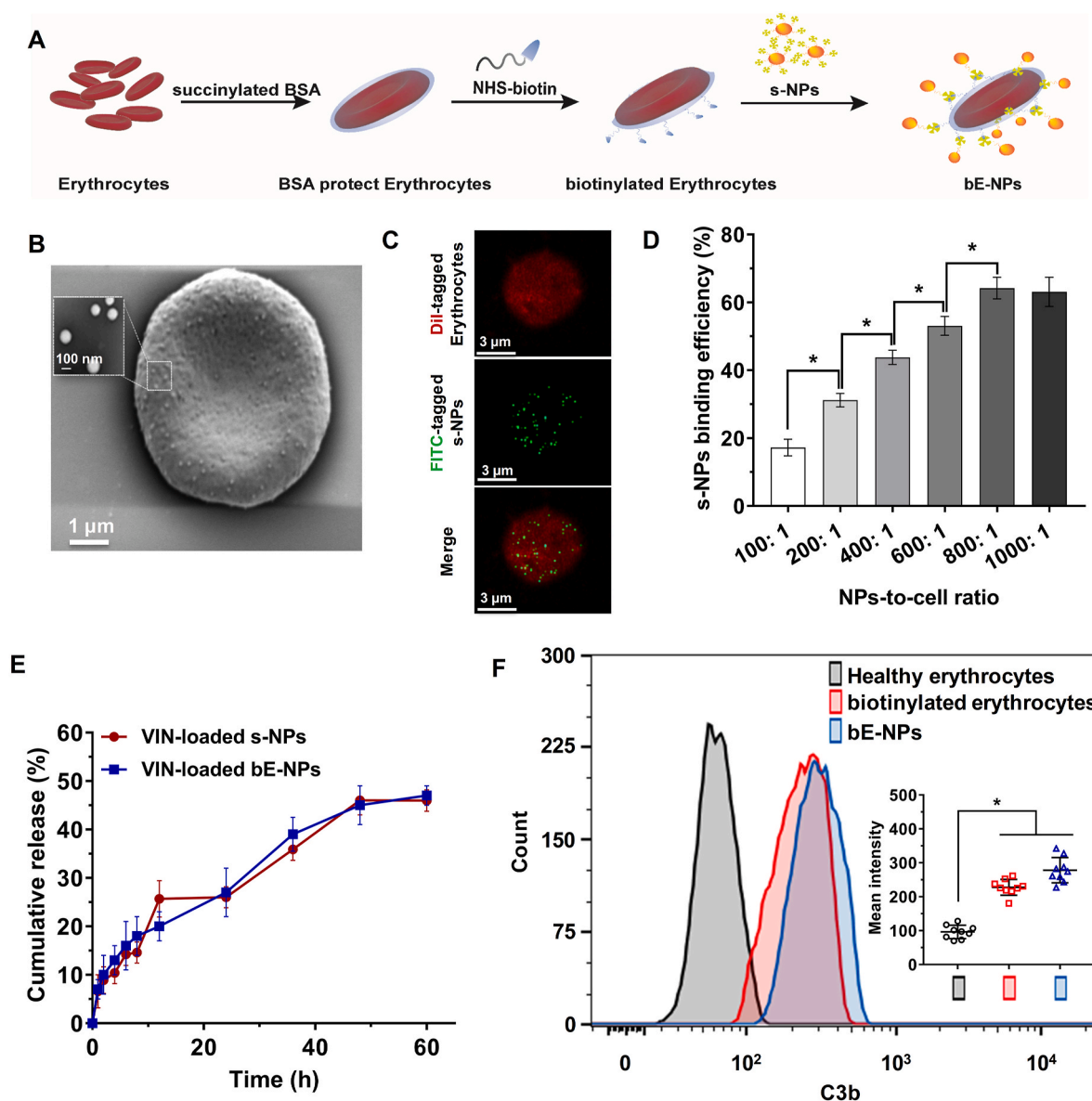After biotinylation of erythrocytes, we evaluated whether the s-NPs

**Fig. 1.** Preparation and characterization of bE-NPs. (A) Schematic of the preparation of bE-NPs. (B) SEM and (C) CLSM images of bE-NPs. (D) Nanoparticle binding efficiency. The data are presented as the means ± SD (n = 3). * indicates P < 0.05. (E) *In vitro* VIN release from s-NPs and bE-NPs in PBS (pH = 7.4) at 37 °C. The data are presented as the means ± SD (n = 3). (F) FCM analysis of C3b in serum depositing and binding on the surface of erythrocytes. *p < 0.05 compared with the Healthy erythrocytes group.

could efficiently assemble onto the biotinylated erythrocytes. To do this, first, we visualized the assembly of s-NPs on the biotinylated erythrocytes using SEM and CLSM. As shown in Fig. 1B and C, these s-NPs indeed assembled on the surface of biotinylated erythrocytes based on both SEM and CLSM. Then, we quantitatively evaluated the binding of s-NPs that linked to biotinylated erythrocytes. The biotinylated erythrocytes were incubated with the FITC-tagged s-NPs in a range of nanoparticle/cell ratios of 100:1 to 1000:1, and the binding efficiency of s-NPs on biotinylated erythrocytes was determined by FCM using FITC fluorescence. As shown in Fig. 1D, the FCM data confirmed the efficient assembly of the s-NPs on the biotinylated erythrocytes. There was a continuous increase in the binding efficiency of s-NPs on biotinylated erythrocytes, with increasing nanoparticle/cell ratios up to 800:1, but with a further increase in the ratio (1000:1), the binding efficiency of s-NPs exhibited no remarkable enhancement, which may be ascribed to the saturation of biotin on the surface of erythrocytes. Therefore, a s-NPs/biotinylated erythrocyte ratio of 800:1 was chosen for subsequent studies.

The *in vitro* VIN release study was performed to examine the influence on drug release properties of the nanosystem after the connection between VIN-loaded s-NPs and biotinylated erythrocytes. As shown in Fig. 1E, the drug release behavior of VIN-loaded bE-NPs was similar to those of VIN-loaded s-NPs, indicating a limited effects on the physico-chemical properties of the nanosystem after the bond of s-NPs with erythrocytes via avidin-biotin method. As a result, the delayed drug release would be beneficial in preventing rapid leakage during the process of drug delivery *in vivo* and therefore increase the accumulation of drug in the targeted sites. The RAW264.7 cells were pre-loaded with VIN-loaded bE-NPs, then washed with phosphate buffered saline (PBS) and incubated in fresh media for different time intervals (0 h, 1 h, 2 h, 4 h, 6 h, 8 h, 12 h, 24 h). Sustained release of VIN from RAW264.7 cells was observed and achieved cumulative release of 12% after 24 h incubation. Meanwhile, a faster release pattern was obtained (25%) in DMEM containing 10% FBS with addition of LPS and IFN-γ (Fig. S4), which indicated that drug release would be accelerated in tumor microenvironment. The release of drugs from macrophages is a

complicated process. Based on the results of our study and previous researches [29,30], the release of VIN from the RAW264.7 cells-hitchhiked bE-NPs would undergo three phases. Firstly, some part of free drugs might be released from bE-NPs within cells, and then diffused into the surroundings via passive driving force caused by concentration gradient between cells and surroundings, or were pumped

out of macrophages by P-gp. When these drug-loaded macrophages reached the inner of tumor tissue which is filled with inflammatory cytokines (simulated by adding LPS and IFN-γ), the macrophages were activated via the bindings with Toll-like receptor 4 and IFN-γ receptor, and then promoting drug release by exocytosis of the prematurely released free drugs within cells and the NPs. Finally, the residuary drugs
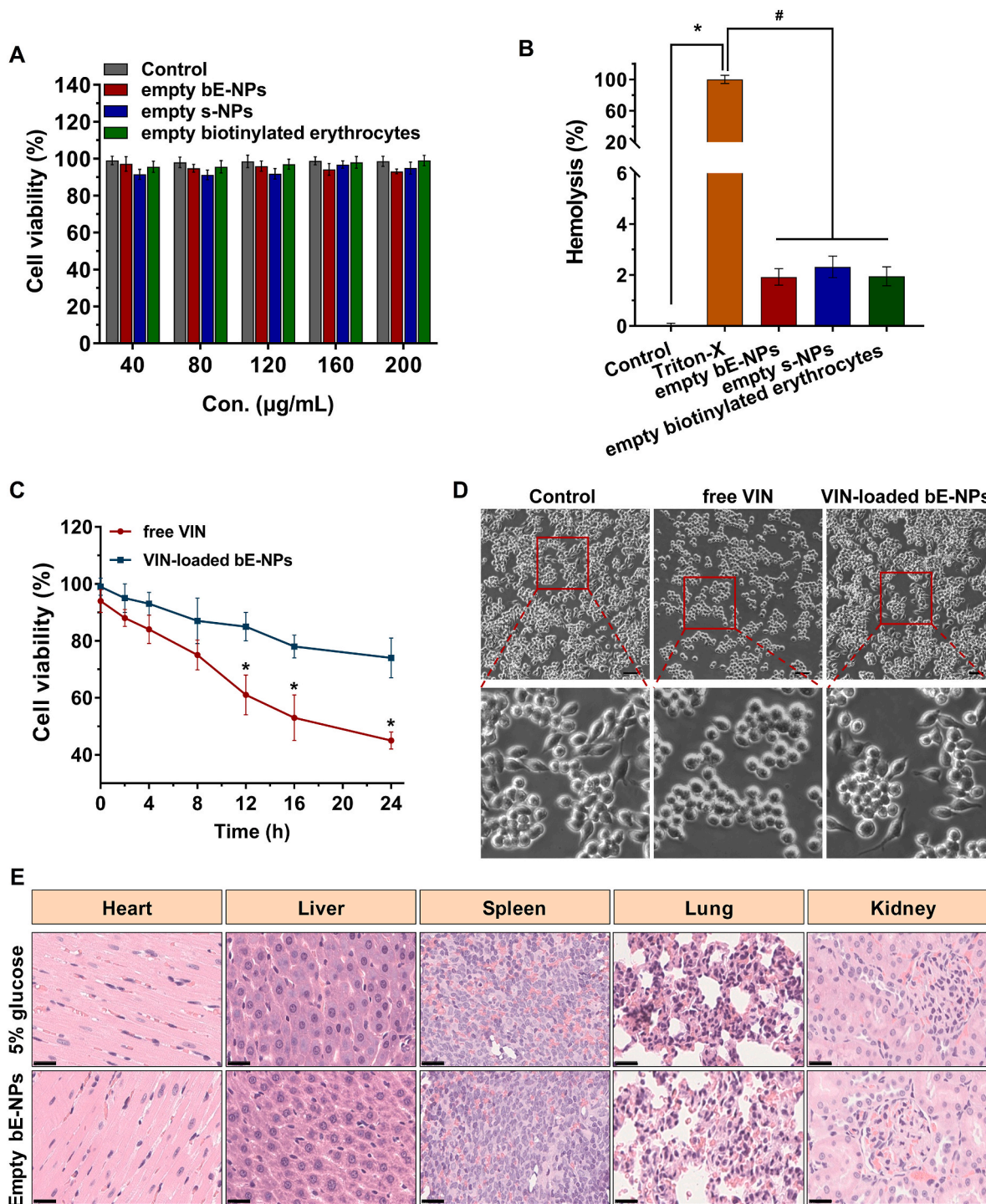


**Fig. 2.** Preliminary safety evaluation of empty bE-NPs. (A) Cell viability of RAW264.7 cells incubated for 72 h with different concentrations of empty formulations. The data are presented as the means ± SD (n = 6). (B) Hemolysis assay of empty formulations. PBS and Triton-X were served as the negative and positive control, respectively. The data are presented as the means ± SD (n = 3). *p < 0.05 compared with the negative control (PBS). #p < 0.05 compared with the positive control (Triton-X). (C) The cytotoxicity of free VIN or VIN-loaded bE-NPs toward RAW264.7 cells. The data are presented as the means ± SD (n = 6). * indicates P < 0.05. (D) Microscopic images of RAW264.7 cells after being hitchhiked by free VIN or VIN-loaded bE-NPs. Scale bars represent 50 μm. (E) Histological staining of organs from healthy rats treated with empty bE-NPs. Scale bars represent 25 μm.

would keep a sustained release from the NPs that were excreted from the activated macrophages.

Evidences showed that C3b-opsonized erythrocytes can be recognized by C3b receptors expressed on the surface of monocytes/macrophages [16]. Under the specific action of C3b-C3b receptors, these kinds of erythrocytes can be readily engulfed by monocytes/macrophages [21, 22]. The biotinylation is considered to mimic the natural property of senescence of erythrocytes with the intervention of complement system related to C3b [21,22]. After the pretreatment with serum, the deposition of C3b on the surface of bE-NPs was quantified by FCM. As shown in Fig. 1F, a significant amount of C3b from the serum was deposited on the surface of biotinylated erythrocytes compared with the healthy erythrocytes, indicating a role of biotinylation to regulate complement activation resulting in the binding of C3b to the surface membrane structure of erythrocytes. With the connection of s-NPs onto biotinylated erythrocytes to form bE-NPs via the specific affinity of streptavidin-biotin, a comparable amount of C3b was deposited on the surface of bE-NPs than that of biotinylated erythrocytes. Thus, bE-NPs are provided with the biological basis as potential carriers for monocytes/macrophages-hitchhiked drug delivery for anticancer treatment *in vivo*.

### 3.2. Preliminary safety test of bE-NPs

In addition to having suitable physiochemical properties, an ideal drug delivery carrier should have minimal toxicity and high biocompatibility. We first conducted cytotoxicity and hemolysis assays on the empty bE-NPs to assess their biocompatibility. As shown in Fig. 2A, the viability of RAW264.7 cells was >90% after incubation with empty bE-NPs for 72 h, revealing that the formulations were relatively safe. Additionally, the percentage of hemolysis increased to about 2.0–2.5% after treatment with empty bE-NPs, empty s-NPs or empty biotinylated erythrocytes, indicating that the formulations are highly blood compatible (less than 5%) (Fig. 2B).

The cytotoxicity of the engulfed VIN-loaded bE-NPs to the monocytes/macrophages as carriers is a key issue for the cell-mediated biomimetic delivery system. The negligible toxicity was validated by a time-dependent MTT assay. As shown in Fig. 2C, with the extension of treatment time of VIN, free VIN could result in obvious cytotoxicities as a time-dependent manner toward RAW264.7 cells, especially after 12 h of processing. In contrast, VIN-loaded bE-NPs showed relatively weaker toxicities than free VIN at the corresponding time points. Furtherly, microscopic results (Fig. 2D) showed that the loading of free VIN caused RAW264.7 cells to get round and detached, so as to inhibit the growth of cells. However, RAW264.7 cells hitchhiked by VIN-loaded bE-NPs still grew well with just limited changes of both the amount and the morphology of cells up to 24 h, which is consistent with the results of MTT (Fig. 2C). These encouraging results indicated that both high bE-NPs loading and low destroying effects to the vehicles (RAW264.7 cells) could be realized simultaneously within the given period of time. In addition, the immunologic characteristics of macrophages of exocytosis in response to stimulation by inflammatory factors were not disturbed by VIN-loaded bE-NPs which hitchhiked in the macrophages (Fig. S4). In fact, VIN-loaded bE-NPs would undergo a gradual and slow drug release process inside the macrophages after phagocytosis (Fig. 1E), thus retarding the damage to the macrophages used as carriers. Meanwhile, a considerable number of the monocytes/maocrophages-hitchhiked bE-NPs could reach the tumor site after 12 h of administration (Fig. 4A), when the rate of cumulative release is about 20% (Fig. 1E). Therefore, the physicochemical properties and biological effects of the designed cell relay-delivery system determine its low toxicity to the carriers in the process of peripheral transport, and then damage the macrophages used as carriers through the time-dependent toxicity after reaching the tumor site, thus releasing drugs to potentially suppress the tumors *in situ*.

For *in vivo* safety assessment, the changes in the body weight of the

tested rats were recorded during the drug treatment period (Fig. S5). No significant difference in the body weight was observed among the tested rats within 7 days. Furthermore, on day 7, tissue sections from the heart, liver, spleen, lung, and kidney were assayed via HE staining after intravenous administration using different samples in healthy rats. As shown in Fig. 2E, compared with the 5% glucose (control) group, no indicators of damage were observed for these organs after treatment, suggesting that empty bE-NPs did not cause systemic toxicity by i.v. injection. Taken together, these results confirmed the low toxicity and good biocompatibility of bE-NPs, possibly due to the biodegradation of the PLGA nanoparticles and the endogenous properties of erythrocytes.

### 3.3. Feasibility of bE-NPs for cell relay-delivered tumor-targeting delivery

One of the challenges in the chemotherapy of solid tumors is the lack of a platform that delivers anticancer drugs to the inner regions. Monocytes/macrophage-mediated delivery of nanomedicines has great potential in solid tumor treatment because it can avoid interception by the immune system and cross the blood vessel barriers to reach tumors. In this study, we used bE-NPs as the carrier to hitchhike on monocytes/macrophages for accumulation of anticancer drugs in solid tumors.

According to the design strategy, when the biotinylation rendered the C3b in serum capable of depositing on the erythrocytes' membrane, the C3b-mediated phagocytosis of the hybrid carriers by macrophages is expected to be enhanced. To verify this hypothesis, the phagocytosis by RAW264.7 cells of various FITC-tagged formulations after pretreating with rat serum or PBS-BSA was conducted. As shown in Fig. 3A, the phagocytosis of FITC-tagged s-NPs by RAW264.7 cells was not significantly influenced by the pretreatment with serum or PBS-BSA, where very similar fluorescence intensities were exhibited. In contrast, serum-pretreated FITC-tagged bE-NPs exhibited stronger intracellular fluorescence than PBS-BSA-pretreated FITC-tagged bE-NPs, which revealed the contribution of C3b in serum to the opsonization of the biotinylated erythrocytes in the bE-NPs for macrophage uptake. Moreover, the phagocytosis of serum-pretreated FITC-tagged bE-NPs was more than that of serum-pretreated or PBS-BSA-pretreated FITC-tagged s-NPs, revealing that serum-pretreated bE-NPs can significantly promote the phagocytosis activity of macrophages. However, the macrophage uptake of PBS-BSA-pretreated FITC-tagged bE-NPs was not ideal, becoming almost equivalent to that of serum-pretreated or PBS-BSA-pretreated FITC-tagged s-NPs. In addition, the blocking of C3b, which is binding on the surface of bE-NPs from the serum, partially suppressed the phagocytosis of bE-NPs by macrophages (Fig. S7). Although the phagocytosis of bE-NPs by RAW264.7 cells was not completely inhibited after the blocking of C3b, the result demonstrated the binding of C3b on the surface of bE-NPs is still one of the indispensable regulators in mediating the process of phagocytosis by macrophages. According to the results in Fig. 1F, all these data indicated that the combination of C3b in serum with the biotinylated erythrocytes can trigger the efficient recognition and phagocytosis of bE-NPs by macrophages, and then potentially committing a further migration of the delivery systems to the tumor sites by the homing effect of macrophages.

To investigate the efficiency of bE-NPs phagocytosed by macrophages, the proportions of serum-pretreated bE-NPs phagocytosed by RAW264.7 cells varying within 24 h were analyzed and gated by FCM. As shown in Fig. 3B, the total amount of bE-NPs was represented by the proportion of erythrocytes in the suspension after the mixture of serum-pretreated bE-NPs and RAW264.7 cells for 0 h (37.68%). With the extension of treatment time, un-phagocytosed bE-NPs represented by the proportion of remaining erythrocytes in the suspensions time-dependently reduced from 37.68% to 1.86% within 24 h, indicating the delivery efficiency of bE-NPs to macrophages is theoretically close to about 95% *in vitro*. Although biotinylated erythrocytes (or bE-NPs) are difficult to achieve long-term circulation *in vivo*, according to the results (Fig. 3B), the delivery efficiency can still reach nearly 50% within 3 h, which confirms the feasibility and efficiency of the monocytes/
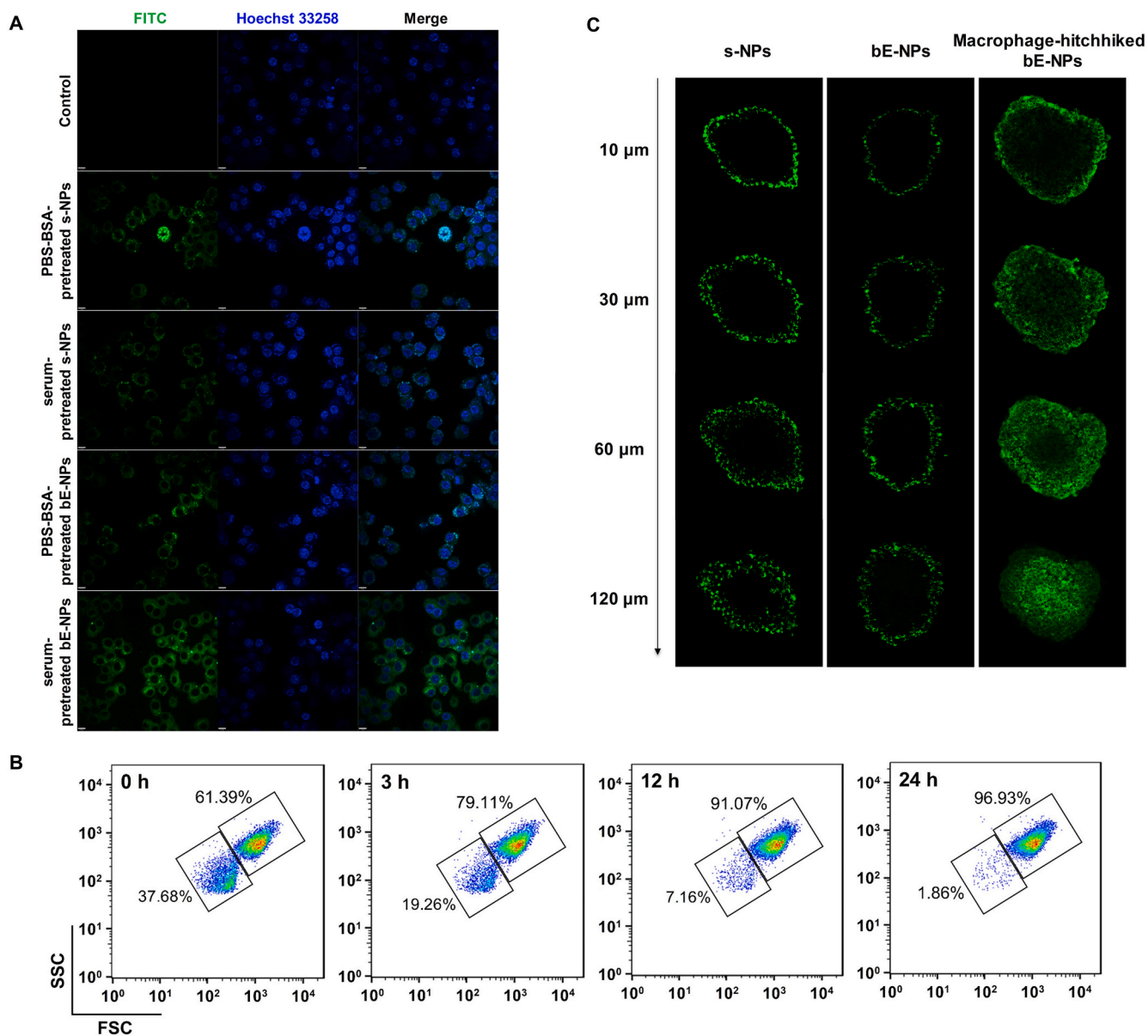
**Fig. 3.** Feasibility of bE-NPs for cell relay-delivered tumor-targeting delivery. (A) Cellular uptake of different FITC-tagged formulations by RAW264.7 cells. Intracellular fluorescence was captured by CLSM. Scale bars represent 10 μm. (B) FCM analysis of the phagocytic efficiency of bE-NPs into RAW264.7 cells from 3 to 24 h. The amount of erythrocytes at 0 h were served as the total of bE-NPs. (C) Z-stack CLSM images of 3D tumor spheroids established by Walker-256 cells after incubation with FITC-tagged s-NPs, bE-NPs or RAW264.7-hitchhiked bE-NPs.

macrophages-hitchhiked delivery strategy of bE-NPs.

Three-dimensional (3D) tumor spheroids have frequently been employed as an ideal *in vitro* platform mimicking solid tumors to predict drug effects. The tumor spheroids are free of blood vessels; therefore, transportation from cell to cell is the only way to reach the core of the tumor spheroids [31]. To test the potential of macrophages to facilitate intratumoral transport of bE-NPs, a 3D tumor spheroid model was built with adherent Walker-256 cells. As shown in Fig. 3C, s-NPs and bE-NPs were hard to penetrate into the depth of the tumor spheroid. However, the macrophage-hitchhiked bE-NPs exhibited obvious penetration within the tumor spheroids compared with others. Considering the characteristics of macrophages to infiltrate tumor spheres, the hitchhiking of macrophages by bE-NPs leads to the capability of the delivery systems to penetrate into the cores of the Walker-256 tumor spheroids. These results demonstrated that macrophages could significantly facilitate the intratumoral accumulation of nanomedicines.

After a series of *in vitro* studies, the biodistribution of DIR-tagged bE-

NPs was photographed by gathering fluorescence signals from Walker-256-bearing rats. Based on whole body imaging (Fig. 4A), DIR-tagged s-NPs possessed a low tumor-targeting ability *in vivo*, which could be attributed to the nanoparticles' lack of selectivity. The results demonstrated that it may be hard for bare nanocarriers to significantly accumulate in the tumor site based on their nanosize alone. In contrast, a higher accumulation of DIR-tagged bE-NPs was detected in the tumor sites, compared with the control DIR-tagged s-NPs group. Enhanced tumor accumulation of DIR-tagged bE-NPs was further confirmed with the images of isolated tumors (Fig. S6). This phenomenon indicted that the introduction of monocytes/macrophages-induced tumor-targeting enhanced bE-NP accumulation in tumors.

To further test the potential of the cell relay-delivery strategy for tumor-targeted delivery, FITC-tagged bE-NPs were used to perform immunofluorescence detection of the tumor. As shown in Fig. 4C and D, a small amount of FITC-tagged s-NPs could enter the tumor tissue, indicating that they resulted in relatively limited accumulation in the
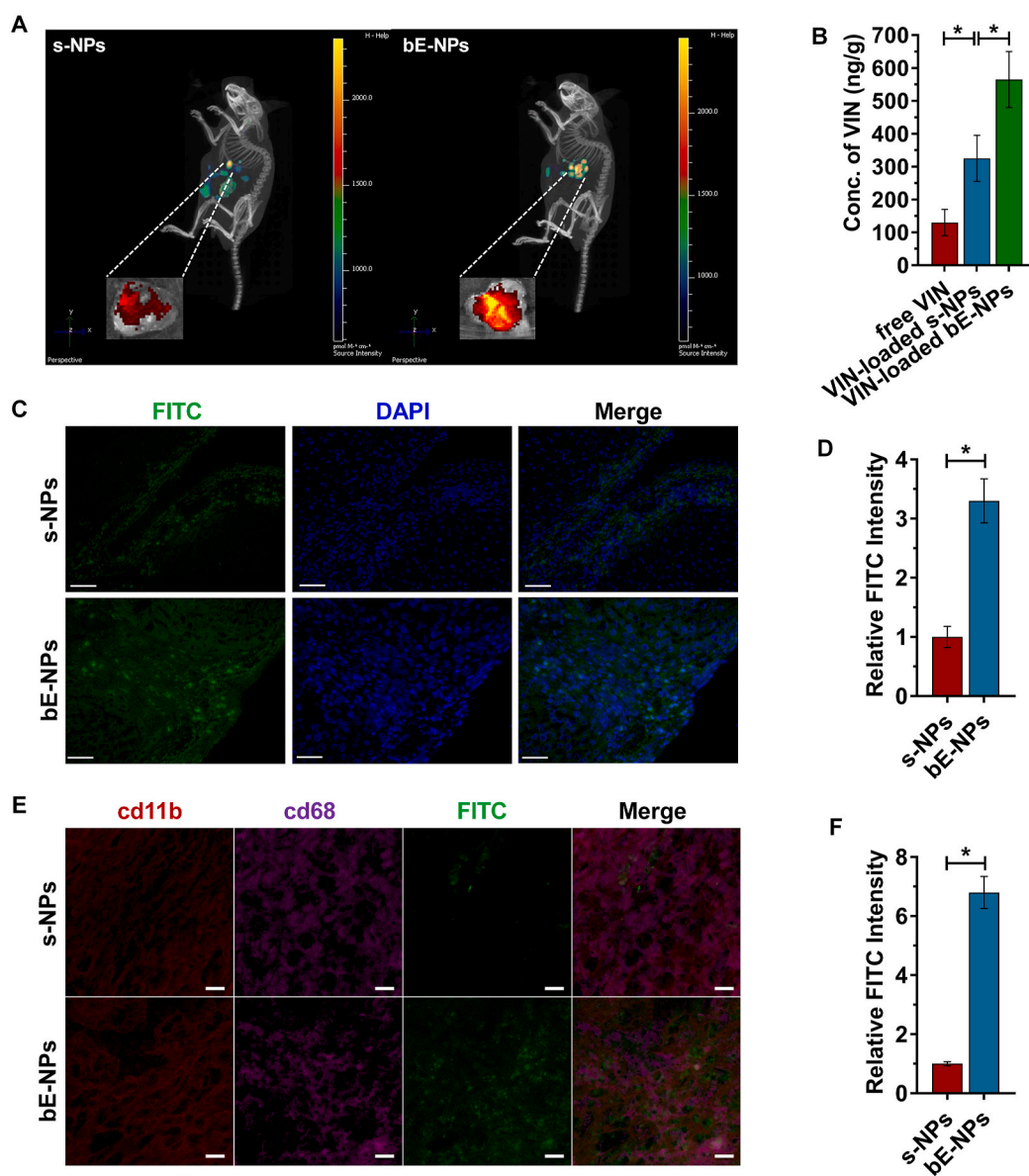
**Fig. 4.** *In vivo* targeting ability test. (A) *In vivo* real-time imaging of different DIR-tagged samples in the tumor showing the biodistribution of nanocarriers in animals and tumor tissues. (B) Concentration of VIN in tumors 12 h after i.v. injection. (C) Distribution of FITC-tagged samples (green) in the tumor of subcutaneous Walker-256-bearing rats determined by fluorescence microscope. The nuclei were stained by DAPI (blue). Scale bars represent 50 μm. (D) Relative fluorescence intensity corresponding to Fig. 4C, n = 3. (E) Fluorescent images of FITC-tagged samples (green) on the site with a tumor penetration depth of 2 mm. Tumor-infiltrated macrophages were stained with anti-CD11b (AlexaFluor 568, shown in red) and anti-CD68 (AlexaFluor 647, shown in violet). Scale bars represent 10 μm. (F) Relative fluorescence intensity corresponding to Fig. 4E, n = 3. * indicates P < 0.05. (For interpretation of the references to colour in this figure legend, the reader is referred to the Web version of this article.)

tumor tissue. The nanoparticles accumulate in the tumor tissue via a passive targeting mechanism known as the enhanced permeability and retention (EPR) effect [32]. However, the EPR effect may not be sufficient to direct the tissue distribution of nanoparticles due to their nonspecific behavior [33]. Therefore, s-NPs resulted in relatively limited tumor-targeted delivery. As we expected, FITC-tagged bE-NPs showed a much higher accumulation than FITC-tagged s-NPs in the tumor region, indicating the precise tumor targeting property of bE-NPs with the hitchhiking of monocytes/macrophages. To further investigate the intratumoral distribution of bE-NPs, and slices of the tumor tissues were prepared, and a middle one was chosen for fluorescence imaging. As shown in Fig. 4E and F, the infiltration of monocytes/macrophages was observed in the internal region of tumor with depth of 2 mm, which was demonstrated by double positive of CD11b and CD68. For FITC-tagged free s-NPs-treated group, only weak and inhomogeneous FITC fluorescence signals can be detected in the selected region, reflecting a limited tumor penetration and retention capacity of free nanoparticles. In contrast, for bE-NPs-treated sample, a stronger FITC signal was evenly distributed in the internal region with monocytes/macrophages infiltration, indicating an efficient intratumoral delivery of monocytes/macrophages-hitchhiked bE-NPs. Combined with the results

in vitro (Fig. 3), selectively phagocytized bE-NPs, mediated by C3b (Fig. S7), were effectively transported to tumor tissues by monocytes/macrophages inspired by the natural trafficking activity to tumor (Fig. 4A-D and Fig. S6). Furtherly, bE-NPs efficiently infiltrated the tumor bulk (Figs. 3C and 4E), which is due to the natural tumor infiltrating ability of monocytes/macrophages. These results provided a proof-of-concept evidence of the efficient intratumoral accumulation of nanotherapeutics achieved by the biotinylated erythrocytes-triggered monocytes/macrophages-hitchhiked delivery system, and emphasized the advantage of the bE-NPs in targeting delivery and infiltration of tumor *in vivo*.

Because a high tumor distribution of the bE-NPs was observed by *in vivo* imaging and immunofluorescence detection, the concentration of VIN in the tumor was assessed in Walker-256-bearing rats to further evaluate the tumor accumulation of bE-NPs (Fig. 4B). The rats were euthanized at 12 h after i.v. injection with different formulations containing VIN, and their tumors were collected. As expected, the concentration of VIN in the tumor of VIN-loaded bE-NPs was 4.3-fold higher than that of free VIN and 1.7-fold higher than that of VIN-loaded s-NPs. The results demonstrated that efficient tumor-targeted delivery of anticancer drugs was achieved by using such a biotinylated erythrocyte-

triggered monocytes/macrophages-hitchhiked delivery system. These *in vivo* results (Fig. 4 and Fig. S6) from tumor model animals agreed with the results of the *in vitro* tumor spheroids shown in Fig. 3C.

Overall, these initial data resulting from *in vitro* (Fig. 3) and *in vivo* (Fig. 4 and Fig. S6) studies provided substantial evidence that bE-NPs have the potential to accomplish specific targeting of payloads to tumors for cell relay-delivered tumor-targeting delivery.

### 3.4. Capability of the bE-NPs for antitumor activity

To further determine whether our hybrid drug delivery system displays antitumor activity *in vivo*, the effects of VIN-loaded bE-NPs on tumor growth inhibition in subcutaneous Walker-256-bearing rats were investigated. As shown in Fig. 5A, the tumor volume of Walker-256-bearing rats administered 5% glucose as a control rapidly increased over 18 days, whereas that of rats administered free VIN, VIN-loaded s-NPs or VIN-loaded bE-NPs displayed tumor inhibition to different extents. Among these groups, the maximal reduction in tumor growth was noted in the group treated with VIN-loaded bE-NPs. This correlated with the abovementioned data revealing the advantage of bE-NPs over the other formulations we tested in tumor spheroid induction *in vitro* (Fig. 3C) and tumor-specific distribution *in vivo* (Fig. 4 and Fig. S6), indicating the advantage of cell relay-delivery. In addition, VIN-loaded s-NPs exhibited moderate improvement in tumor inhibition compared with VIN-loaded bE-NPs, which could be attributed to the insufficient tumor-targeting ability of bare nanocarriers.

Immunohistochemical analysis was conducted after the achievement of tumor inhibition data. As shown in Fig. 5B and C, immunohistochemistry of CD31 in tumors after treatment showed that compared with the other treatments, VIN-loaded bE-NP treatment resulted in a larger area of apoptosis. The normal 5% glucose group, free VIN group, and VIN-loaded s-NPs group showed dense cellular tissues. The above findings indicate that VIN-loaded bE-NPs exert stronger antitumor activity than other formulations. The tendency found in the

immunohistochemical analysis was in accordance with the findings of the distribution *in vivo* (Fig. 4 and Fig. S6) and the tumor growth inhibition *in vivo* (Fig. 5A).

The clinical therapeutic benefits are mainly determined based on the quality of life and prolonged survival time of patients with cancer. In a further investigation of the potential of VIN-loaded bE-NPs in antitumor therapy *in vivo*, the Kaplan-Meier survival curve of subcutaneous Walker-256-bearing rats was used after the tumor growth inhibition studies. As shown in Fig. 5D, treatment with VIN-loaded bE-NPs significantly prolonged the median survival time (46.5 days), which was 1.5-, 1.4-, and 1.2-fold higher than that of 5% glucose, free VIN and VIN-loaded s-NPs, respectively. Both the P values (vs 5% glucose group) of the free VIN group ($p = 0.3688$) and the VIN-loaded s-NPs group ($p = 0.0835$) demonstrate the ineffectiveness in improving the survivals of these tumor-bearing rats, although the median survivals are extended. However, the P value of VIN-loaded bE-NPs group ($p = 0.0456$) show a statistical improving of the survival than any other groups. The tendency found above agreed with the finding of the tumor growth inhibition (Fig. 5A). This was mainly attributed to the cell relay-delivered tumor-targeting delivery of bE-NPs, which was demonstrated by *in vitro* (Fig. 3) and *in vivo* (Fig. 4 and Fig. S6) studies.

In the inner regions of solid tumors, the blood and lymphatic vessels are greatly compressed due to the rapid proliferation of peripheral tumor cells, thereby producing a high-pressure, hypoxic, acidified and necrotic environment in solid tumors [34]. Because of a lack of penetrating ability, it could be very difficult for free anticancer drugs to accumulate in the inner regions of solid tumors through a passive diffusion process. Bare NPs also could not penetrate deeper into the tumor to kill the tumor cells based on their nanosize alone. Therefore, tumor cells in the inner regions of solid tumors are resistant to chemotherapy, posing great challenges to cancer treatments [35]. To enhance the concentration of therapeutics in the center of a solid tumor, the cell relay-delivery strategy was developed in this study. We applied VIN-loaded bE-NPs, as the vector to achieve *in vivo*
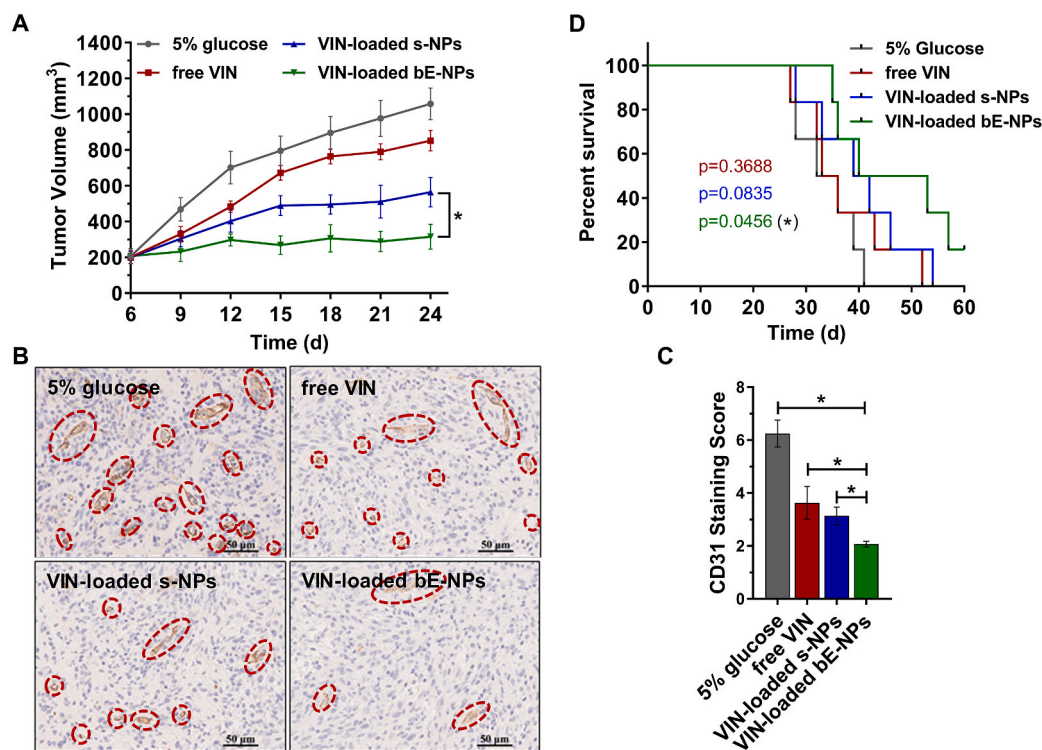


**Fig. 5.** Antitumor effects of drug-loaded bE-NPs *in vivo*. (A) Tumor growth curves, (B) immunohistochemistry of CD31 in tumors, (C) the semi-quantitative analysis of CD31 by staining score and (D) Kaplan-Meier survival curves of subcutaneous Walker-256-bearing rats following different treatments. Log-rank test compared with 5% glucose group is to estimate the probability of survival in statistics. The data are presented as the means ± SD (n = 6). * indicates P < 0.05.

monocytes/macrophages-specific loading of VIN according to the biomimetic strategy. With enhanced intratumoral accumulation by the natural trafficking activity of monocytes/macrophages (Figs. 3C and 4), the capacity of VIN-loaded bE-NPs for chemotherapy was improved compared with free VIN and VIN-loaded s-NPs in subcutaneous Walker-256-bearing rats (Fig. 5).

The goal for a DDS is to achieve optimal therapeutic efficacy with acceptable safety profiles during *in vivo* applications. As a proof-of-principle demonstration, herein, the body weight variation of tumor model animals was monitored during the experimental period. As shown in Fig. 6A, greater than 9% weight loss was detected in the free VIN-treated group at the end of the experimental period. The weight loss of the free VIN group was likely due to the toxicity of VIN and tumor cachexia. Moreover, hemogram analysis was performed to further evaluate the *in vivo* safety properties of the nanocarriers. As shown in Fig. 6B and C, there was no obvious decrease in the red blood cell (RBC) and white blood cell (WBS) levels in the VIN-loaded bE-NPs and VIN-loaded s-NPs, respectively. However, the mean corpuscular volume (MCV) of the free VIN group was significantly lower than that of the other two groups (Fig. 6D). As shown in Fig. 6E, free VIN displayed
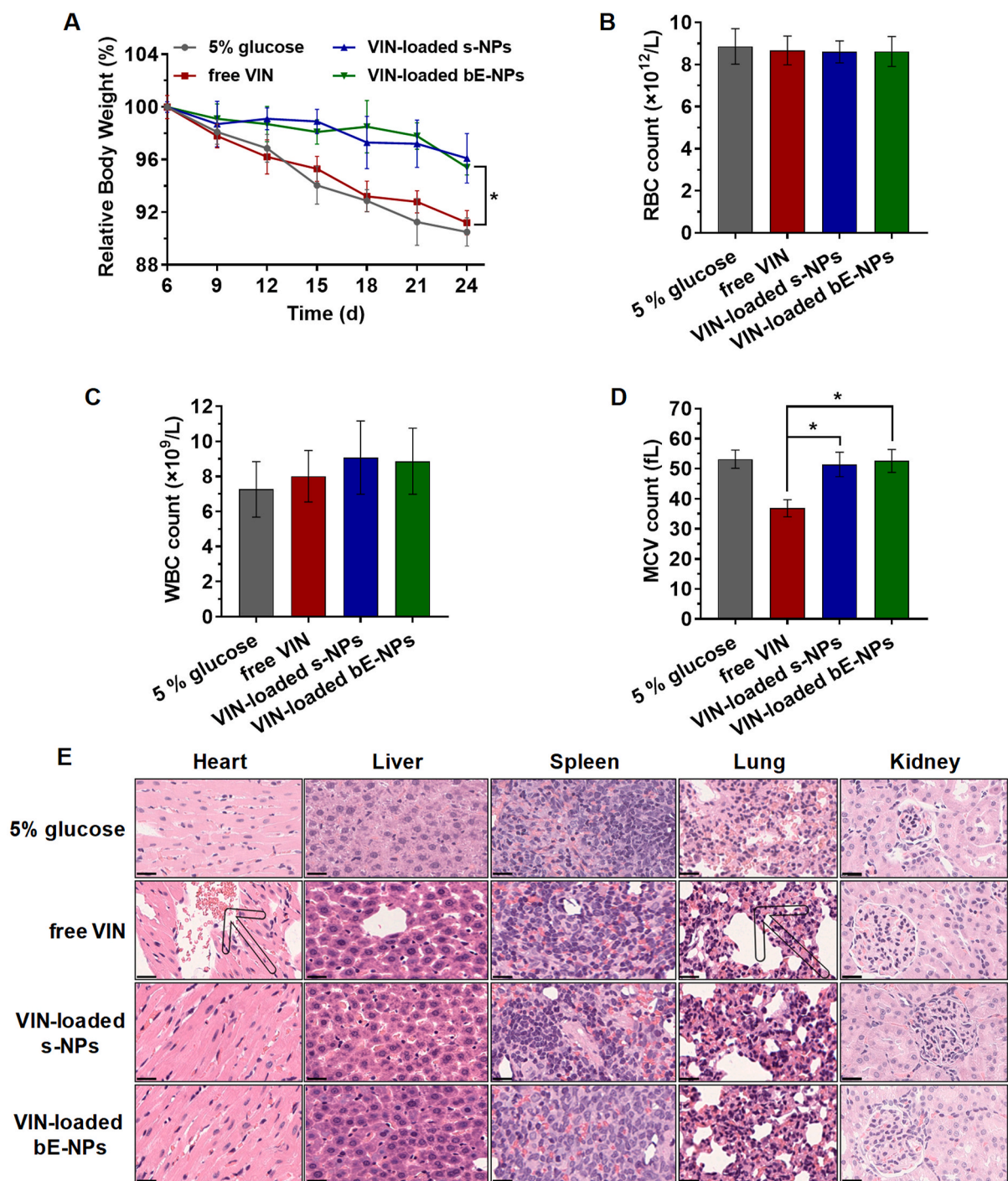


**Fig. 6.** *In vivo* safety evaluation in subcutaneous Walker-256-bearing rats. (A) Body weight changes. Hematological indicators of (B) RBC, (C) WBC and (D) MCV. (E) HE staining of major organ sections after various treatments. The data are presented as the means ± SD (n = 6). * indicates $P < 0.05$ compared with the free VIN group.

histological damage in the heart and lung, while the VIN-loaded s-NPs only displayed mild liver toxicity. In contrast, no indicators of damage were observed in the main organs after treatment with VIN-loaded bE-NPs. These results demonstrated that bE-NPs largely alleviated the toxicity of VIN as determined from the negligible weight loss, hematological indicators and histological staining of organs and were relatively safe at the test dose. In the clinic, many current chemotherapeutic drugs such as VIN often cause severe side effects due to their production of a similar cytotoxicity in both cancerous and healthy cells. To overcome this challenge, several different types of DDSs have been developed by many researchers. The rationale behind this approach is to increase antitumor efficacy while reducing systemic side effects. Herein, these above results indicated that the hybrid DDSs reduced unspecific cellular uptake through the cell relay-delivered tumor-targeting delivery.

Overall, the above findings indicate that VIN-loaded bE-NPs exert stronger antitumor activity than other formulations in cells and mouse tumor models. These *in vitro* and *in vivo* results are consistent with previous findings, suggesting the superiority of bE-NPs investigated for the physiochemical properties (Fig. 1, Fig. S1, Fig. S2 and Fig. S3), safety (Fig. 2, Fig. S5 and Fig. 6), tumor targeting (Figs. 3C and 4 and Fig. S6), and antitumor activity (Fig. 5). The cells-mediated hybrid DDSs are a potential therapeutic candidate to treat solid tumors.

## 4. Conclusion

In this study, bE-NPs, drug-loaded biodegradable nanoparticles assembling on erythrocytes using avidin-biotin coupling, were developed to achieve accumulation of anticancer drugs in tumors according to the strategy of cell relay-delivery. After encapsulating the model drug (VIN), drug-loaded bE-NPs could effectively enhance the antitumor efficacy *in vitro* and *in vivo* compared with using the drug-loaded nanoparticles alone. Although preliminary, the research data of this work collectively suggest that bE-NPs might provide a promising intravenous tumor-targeted delivery platform for solid tumor treatment. In a future study, we will perform *in vitro* and *in vivo* studies examining the targeted delivery mechanism and further explore the application of bE-NPs in oncotherapy.

## CRediT authorship contribution statement

**Ye Feng:** Methodology, Validation, Investigation, Data curation. **Qianqian Liu:** Formal analysis, Investigation, Data curation. **Yi Li:** Conceptualization, Methodology, Software, Validation, Formal analysis, Investigation, Data curation, Writing - original draft, Writing - review & editing, Visualization, Supervision, Project administration. **Yang Han:** Formal analysis, Data curation. **Meng Liang:** Formal analysis, Investigation. **Hao Wang:** Formal analysis. **Qing Yao:** Formal analysis. **Yuli Wang:** Formal analysis. **Meiyan Yang:** Formal analysis. **Zhiping Li:** Formal analysis. **Wei Gong:** Formal analysis. **Yang Yang:** Conceptualization, Writing - original draft, Writing - review & editing, Supervision, Project administration, Funding acquisition. **Chunsheng Gao:** Supervision, Project administration, Funding acquisition.

## Declaration of competing interest

We declare that we have no financial and personal relationships with other people or organizations that can inappropriately influence our work. There is no professional or other personal interest of any nature or kind in any product, service and/or company that could be construed as influencing the position presented in, or the review of the manuscript entitled "Cell relay-delivery improves targeting and therapeutic efficacy in tumors".

## Acknowledgments

## Appendix A. Supplementary data

Supplementary data related to this article can be found at https://doi.org/10.1016/j.bioactmat.2020.11.014.

## References

[1] P. de la Torre, M.J. Perez-Lorenzo, A. Alcazar-Garrido, A.I. Flores, Cell-based nanoparticles delivery systems for targeted cancer therapy: lessons from anti-angiogenesis treatments, Molecules 25 (3) (2020).

[2] P. Allavena, A. Sica, G. Solinas, C. Porta, A. Mantovani, The inflammatory micro-environment in tumor progression: the role of tumor-associated macrophages, Crit. Rev. Oncol.-Hematol. 66 (1) (2008) 1–9.

[3] A. Mantovani, T. Schioppa, C. Porta, P. Allavena, A. Sica, Role of tumor-associated macrophages in tumor progression and invasion, Canc. Metastasis Rev. 25 (3) (2006) 315–322.

[4] M.R. Choi, K.J. Stanton-Maxey, J.K. Stanley, C.S. Levin, R. Bardhan, D. Akin, et al., A cellular Trojan horse for delivery of therapeutic nanoparticles into tumors, Nano Lett. 7 (12) (2007) 3759–3765.

[5] G.A. Dekaban, A.M. Hamilton, C.A. Fink, B. Au, S.N. de Chickera, E.J. Ribot, et al., Tracking and evaluation of dendritic cell migration by cellular magnetic resonance imaging, Wiley Interdiscip. Rev. Nanomed. Nanobiotechnol. 5 (5) (2013) 469–483.

[6] A. Aderem, D.M. Underhill, Mechanisms of phagocytosis in macrophages, Annu. Rev. Immunol. 17 (1999) 593–623.

[7] E. Blanco, H. Shen, M. Ferrari, Principles of nanoparticle design for overcoming biological barriers to drug delivery, Nat. Biotechnol. 33 (9) (2015) 941–951.

[8] H.L. Herd, K.T. Bartlett, J.A. Gustafson, L.D. McGill, H. Ghandehari, Macrophage silica nanoparticle response is phenotypically dependent, Biomaterials 53 (2015) 574–582.

[9] T. Tanei, F. Leonard, X.W. Liu, J.F. Alexander, Y. Saito, M. Ferrari, et al., Redirecting transport of nanoparticle albumin-bound paclitaxel to macrophages enhances therapeutic efficacy against liver metastases, Canc. Res 76 (2) (2016) 429–439.

[10] J. Key, A.L. Palange, F. Gentile, S. Aryal, C. Stigliano, D. Di Mascolo, et al., Soft discoidal polymeric nanoconstructs resist macrophage uptake and enhance vascular targeting in tumors, ACS Nano 9 (12) (2015) 11628–11641.

[11] Y.H. Pei, Y. Yeo, Drug delivery to macrophages: challenges and opportunities, J. Contr. Release 240 (2016) 202–211.

[12] J.J. Fu, D. Wang, D. Mei, H.R. Zhang, Z.Y. Wang, B. He, et al., Macrophage mediated biomimetic delivery system for the treatment of lung metastasis of breast cancer, J. Contr. Release 204 (2015) 11–19.

[13] L.Y. Zheng, X.X. Hu, H. Wu, L.T. Mo, S.T. Xie, J. Li, et al., Vivo monocyte/macrophage-hitchhiked intratumoral accumulation of nanomedicines for enhanced tumor therapy, JACS 142 (1) (2020) 382–391.

[14] R.P. Taylor, C.J. Reist, W.M. Sutherland, A. Otto, R.H. Labuguen, E.L. Wright, Invivo binding and clearance of circulating antigen by bispecific heteropolymer-mediated binding to primate erythrocyte complement receptor, J. Immunol. 148 (8) (1992) 2462–2468.

[15] R.P. Taylor, W.M. Sutherland, C.J. Reist, D.J. Webb, E.L. Wright, R.H. Labuguen, Use of heteropolymeric monoclonal-antibodies to attach antigens to the C3b receptor of human erythrocytes - a potential therapeutic treatment, Proc. Natl. Acad. Sci. U.S.A. 88 (8) (1991) 3305–3309.

[16] K. Ganguly, T. Krasik, S. Medinilla, K. Bdeir, D.B. Cines, V.R. Muzykantov, et al., Blood clearance and activity of erythrocyte-coupled fibrinolytics, J. Pharmacol. Exp. Therapeut. 312 (3) (2005) 1106–1113.

[17] C.G. Millan, M.L.S. Marinero, A.Z. Castaneda, J.M. Lanao, Drug, enzyme and peptide delivery using erythrocytes as carriers, J. Contr. Release 95 (1) (2004) 27–49.

[18] A.G. Bajpayee, C.R. Wong, M.G. Bawendi, E.H. Frank, A.J. Grodzinsky, Avidin as a model for charge driven transport into cartilage and drug delivery for treating early stage post-traumatic osteoarthritis, Biomaterials 35 (1) (2014) 538–549.

[19] T. Suzuki, G.L. Dale, Biotinylated erythrocytes - invivo survival and invitro recovery, Blood 70 (3) (1987) 791–795.

[20] F. Turrini, P. Arese, Y. Jie, P.S. Low, Clustering of integral membrane-proteins of the human erythrocyte-membrane stimulates autologous igg binding, complement deposition, and phagocytosis, J. Biol. Chem. 266 (35) (1991) 23611–23617.

[21] D. Bratosin, J. Mazurier, J.P. Tissier, J. Estaquier, J.J. Huart, J.C. Ameisen, et al., Cellular and molecular mechanisms of senescent erythrocyte phagocytosis by macrophages, Rev. Biochim. 80 (2) (1998) 173–195.

[22] Y. Gottlieb, O. Topaz, L.A. Cohen, L.D. Yakov, T. Haber, A. Morgenstern, et al., Physiologically aged red blood cells undergo erythrophagocytosis in vivo but not in vitro, Haematol. Hematol. J. 97 (7) (2012) 994–1002.

[23] T.M. Fahmy, J.P. Schneck, W.M. Saltzman, A nanoscopic multivalent antigen-presenting carrier for sensitive detection and drug delivery to T cells, Nanomed. Nanotechnol. Biol. Med. 3 (1) (2007) 75–85.

[24] Y. Han, X. Chu, L. Cui, S. Fu, C. Gao, Y. Li, et al., Neuronal mitochondria-targeted therapy for Alzheimer's disease by systemic delivery of resveratrol using dual-modified novel biomimetic nanosystems, Drug Deliv. 27 (1) (2020) 502–518.

[25] Y. Han, C. Gao, H. Wang, J. Sun, M. Liang, Y. Feng, et al., Macrophage membrane-coated nanocarriers Co-Modified by RVG29 and TPP improve brain neuronal mitochondria-targeting and therapeutic efficacy in Alzheimer's disease mice, Bioactive Mater. 6 (2) (2021) 529–542.

[26] M.J. Ernsting, W.L. Tang, N.W. MacCallum, S.D. Li, Preclinical pharmacokinetic, biodistribution, and anti-cancer efficacy studies of a docetaxel-carboxymethylcellulose nanoparticle in mouse models, Biomaterials 33 (5) (2012) 1445–1454.

[27] R. Guilhaumou, C. Solas, A. Rome, M. Giocanti, N. Andre, B. Lacarelle, Validation of an electrospray ionization LC/MS/MS method for quantitative analysis of vincristine in human plasma samples, J. Chromatogr. B Anal. Technol. Biomed. Life Sci. 878 (3–4) (2010) 423–427.

[28] Z.L. Chai, D.N. Ran, L.W. Lu, C.Y. Zhan, H.T. Ruan, X.F. Hu, et al., Ligand-modified cell membrane enables the targeted delivery of drug nanocrystals to glioma, ACS Nano 13 (5) (2019) 5591–5601.

[29] Y. Tao, M. Ning, H. Dou, A novel therapeutic system for malignant glioma: nanoformulation, pharmacokinetic, and anticancer properties of cell-nano-drug delivery, Nanomedicine 9 (2) (2013) 222–232.

[30] L. Pang, J. Qin, L. Han, W. Zhao, J. Liang, Z. Xie, et al., Exploiting macrophages as targeted carrier to guide nanoparticles into glioma, Oncotarget 7 (24) (2016) 37081–37091.

[31] G. Mehta, A.Y. Hsiao, M. Ingram, G.D. Luker, S. Takayama, Opportunities and challenges for use of tumor spheroids as models to test drug delivery and efficacy, J. Contr. Release 164 (2) (2012) 192–204.

[32] J. Fang, H. Nakamura, H. Maeda, The EPR effect: unique features of tumor blood vessels for drug delivery, factors involved, and limitations and augmentation of the effect, Adv. Drug Deliv. Rev. 63 (3) (2011) 136–151.

[33] K. Greish, Enhanced permeability and retention of macromolecular drugs in solid tumors: a royal gate for targeted anticancer nanomedicines, J. Drug Target. 15 (7–8) (2007) 457–464.

[34] M. Stohrer, Y. Boucher, M. Stangassinger, R.K. Jain, Oncotic pressure in solid tumors is elevated, Canc. Res 60 (15) (2000) 4251–4255.

[35] H. Yasuda, Solid tumor physiology and hypoxia-induced chemo/radio-resistance: novel strategy for cancer therapy: nitric oxide donor as a therapeutic enhancer, Nitric Oxide Biol. Chem. 19 (2) (2008) 205–216.

[36] Chen J, He H, Li S, Shen Q, An HPLC method for the pharmacokinetic study of vincristine sulfate-loaded PLGA-PEG nanoparticle formulations after injection to rats, J. Chromatogr. B, 2011, 879(21):1967-1972 , 10.1016/j.jchromb.2011.05.031, PMID: 21665557.